Improved Detection of Optically Thin Cirrus Clouds in Nighttime Multispectral Meteorological Satellite Imagery Using Total Integrated Water Vapor Information

KEITH D. HUTCHISON* AND KENNETH R. HARDY†

Center for Remote Environmental Sensing Technology (CREST), Lockheed Missiles and Space Company, Inc (LMSC) Austin Division, Austin, Texas

BO-CAI GAO

University Space Research Association, NASA Goddard Space Flight Center, Greenbelt, Maryland

(Manuscript received 8 March 1994, in final form 4 October 1994)

ABSTRACT

The accurate identification of optically thin cirrus clouds in global meteorological satellite imagery by automated cloud analysis algorithms is critical to environmental remote sensing studies, such as those related to climate change. While significant improvements have been realized with the arrival of multispectral, meteorological satellite imagery, collected by NOAA's Advanced Very High Resolution Radiometer (AVHRR), difficulties can be encountered when attempting to make pixel-level cloud decisions over large and diverse geographic areas found around the globe. These problems are due, in part, to the effects of atmospheric attenuation on cloud spectral signatures, caused primarily by variations in water vapor, since the signatures of water vapor and optically thin cirrus are similar in the nighttime AVHRR infrared channels. In this paper, the authors describe an improved thin-cirrus detection technique that uses the brightness temperature differences between AVHRR channel 3 and channel 5 along with total integrated water vapor information. It is concluded that algorithms must accurately compensate for the impact of water vapor on cloud spectral signatures for enhanced detection of optically thin cirrus clouds in nighttime AVHRR imagery.

1. Introduction

Numerous articles have appeared in recent years to describe methods for conducting automated cloud analyses from multispectral imagery, including bispectral threshold techniques, statistical (spectral) methods, textural analyses, and the application of neural network technology (Inoue 1985; Coakley and Bretherton 1982; Lameii et al. 1994; Key et al. 1989). While there is justification for each approach, the bispectral threshold techniques are most commonly used in operational cloud analysis algorithms, including global cloud analyses performed by the National Oceanic and Atmospheric Administration (NOAA) with the CLAVR [clouds from Advanced Very High Resolution Radiometer (AVHRR)] algorithm (Stowe et al. 1991) as well as the Swedish Meteorological and Hydrological Institute (SMHI) model for regional cloud analyses (Karlsson and Liljas 1990).

One notable work published on bispectral threshold techniques was that of Saunders and Kriebel (1988, hereafter referred to as SK). Their methodology applies a series of simplistic tests that examine variations in AVHRR channels to determine the presence or absence of clouds. Decisions as to whether a pixel is classified as cloud contaminated or cloud-free are based primarily upon the magnitude of differences and ratios between brightness temperatures in two of the multispectral channels. In general, each test employs a specific single-valued threshold to make cloud/no-cloud decisions. The pixel is identified as cloud contaminated if the threshold is exceeded; otherwise, another cloud test is applied. Only when the pixel successfully passes all cloud tests is it classified as cloud-free.

Difficulties can be encountered when attempting to make pixel-level cloud decisions using bispectral techniques over large and diverse geographic areas found around the globe. This problem is due, in part, to the effects of atmospheric attenuation on cloud spectral signatures, caused primarily by variations in water vapor. Under dry, cloud-free conditions, little variation may be observed between the brightness temperatures in AVHRR channels centered near 3.7 μm (channel 3), 11 μm (channel 4), and 12 μm (channel 5) for a blackbody surface. However, as atmospheric moisture increases, the brightness temperature in channel 5 typ-

* Also affiliated with the Center for Space Research, University of Texas, Austin, Texas.

† LMSC Research and Development Division, Palo Alto, California.

Corresponding author address: Dr. Keith D. Hutchison, LMSC Austin Division, Austin, TX 78760.

ically becomes colder than channel 4, since atmospheric attenuation is greater at 12 μm than at 11 μm and the brightness temperatures in channel 4 become less than channel 3 (Hutchison et al. 1991). Brightness temperature variations at the nadir scan position may lie between 0° and 7°C in these channels, depending on the concentration of atmospheric water vapor within the sensor field of view. Similarly, optically thin cirrus absorbs energy more strongly in channel 5 than channel 4 and least in channel 3. Brightness temperature differences for thin cirrus have been observed in the 0°–20° range, depending upon atmospheric attenuation and the emissivity of cirrus clouds (Inoue 1987). Clearly, an accurate treatment of atmospheric water vapor is essential for the analysis of optically thin cirrus in nighttime imagery.

In this paper, we present a multivalued threshold function for the analysis of optically thin cirrus clouds by automated cloud detection algorithms under a wide range of atmospheric moisture conditions. Using the channel 3 minus channel 5 brightness temperature difference (BTD35) in nighttime AVHRR imagery and nearly coincident measurements of columnar total integrated water vapor ($TIWV_c$), obtained from radiosondes then corrected for pathlength of the satellite-viewing geometry ($TIWV_p$), we show that the threshold function separating cloud-free and cirrus cloudy pixels is well defined. Furthermore, we show that this threshold function provides improved sensitivity over the thin cirrus test of SK, which classifies the pixel as cloud contaminated if the channel 4 minus channel 5 brightness temperature difference (BTD45) exceeds a threshold that depends upon satellite viewing geometry and the brightness temperature in channel 4. The improved sensitivity of the threshold function methodology using $TIWV_p$ information is then demonstrated in an automated cloud analysis algorithm.

2. Background

a. Infrared radiative transfer theory

For environmental satellites in low earth orbit, the atmosphere may be represented as a series of horizontal planes of infinite length, known as the plane-parallel atmosphere approximation (Liou 1980). If the satellite imager observes a narrow cone in the local vertical so that everywhere within the cone the cosine of the emergent angle is unity, the monochromatic upwelling radiance for a cloud-free atmosphere, including the surface reflection of downwelling atmospheric radiation, is given in pressure coordinates by Eq. (1), where p_s is the surface pressure and zero is the pressure at the top of the atmosphere:

$$I_\nu(0) = \epsilon_\nu B_\nu(T_s)T_\nu(p_s) + \int_{p_s}^{0} B_\nu[T(p)]\frac{\partial T_\nu(p)}{\partial p}\,dp + (1-\epsilon_\nu)\int_0^{p_s} B_\nu[T(p)]\frac{\partial T_\nu(p)}{\partial p}\,dp, \quad (1)$$

where $B_\nu[T(p)]$ is the Planck function at wavenumber ν, temperature T, and pressure p, e_ν is the emissivity of the surface at wavenumber ν, $T_\nu(p_s)$ is the atmospheric transmittance between surface and space, $I_\nu(0)$ is the radiance arriving at the satellite for wavenumber ν, and T_s is the surface temperature.

The monochromatic transmittance is defined in Eq. (2):

$$T_\nu(p) = \exp\left[-\frac{1}{g}\int_0^p k_\nu(p)q(p)dp\right], \quad (2)$$

where $k_\nu(p)$ is absorption coefficient of the atmosphere at wavenumber ν, $q(p)$ is the mixing ratio of the absorbing gas (q), and g is the acceleration due to gravity. Note that the term $\partial T_\nu(p)/\partial p$ is referred to as the "weighting function," which yields the contribution of monochromatic energy to the upwelling radiance, when multiplied by the Planck function, that originates from each plane.

In reality, monochromatic radiation does not exist because of line broadening from natural, pressure (collision), and Doppler (thermal velocity) effects. Also, since an instrument can distinguish only a finite bandwidth, the upwelling radiance measured by the satellite is integrated over the sensor transmission filter, which is also called the sensor response function, and is given by Eq. (3):

$$I_{\bar\nu}(0) = \frac{1}{\int_{\nu_1}^{\nu_2}\theta(\bar\nu,\nu)d\nu} \times\left[\int_{\nu_1}^{\nu_2}\theta(\bar\nu,\nu)e_\nu B_\nu(T_s)T_\nu(ps)d\nu + \int_{\nu_1}^{\nu_2}\theta(\bar\nu,\nu)\int_{p_s}^{0}B_\nu[T(p)]\frac{\partial T_\nu(p)}{\partial p}dpd\nu + \int_{\nu_1}^{\nu_2}\theta(\bar\nu,\nu)(1-e_\nu)\int_0^{p_s}B_\nu[T(p)]\times\frac{\partial T_\nu(p)}{\partial p}dpd\nu\right], \quad (3)$$

where $\theta(\bar\nu,\nu)$ is the filter (sensor) response function, (ν_1,ν_2) is the wavenumber range of the filter response, and $\bar\nu$ is the filter reference (central) wavenumber. Thus, in general, the energy collected by the satellite depends upon 1) the atmospheric temperature and transmittance profiles, 2) the sensor bandpass filter, and 3) the surface emissivity, while the transmittance profile is, in addition, a function of the physical composition of the atmosphere (e.g., amount of gaseous absorbers and the location of the attenuating medium in the atmosphere). Water vapor is the gas most strongly attenuating the upwelling radiance in the nighttime AVHRR imagery, as shown in Fig. 1, and is known to be highly variably in space and time.

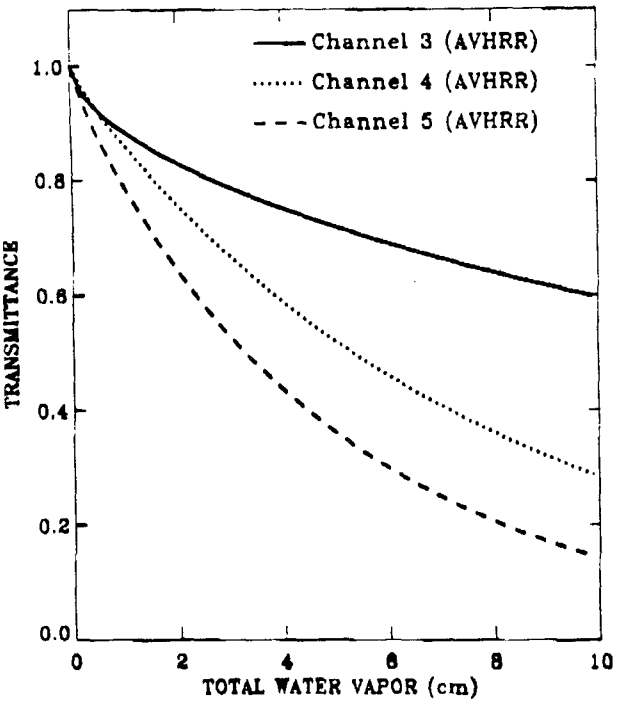

FIG. 1. Transmittance of nighttime *NOAA-11* AVHRR channels 3, 4, and 5 for a cloud-free atmosphere as a function of total integrated water vapor. Transmittances are calculated using LOWTRAN 7 (Kneizys et al. 1988) and averaged between full width at half maximum of AVHRR channels, with the water vapor profile scaled by different factors.

Therefore, it is necessary to compensate for variations of $TIWV_p$ and its effect on upwelling radiance in AVHRR nighttime channels for the accurate analyses of optically thin cirrus clouds.

b. *Correction for atmospheric pathlength dependencies (i.e., limb-darkening effects)*

Since the AVHRR electro-optical imager employs a nadir scan geometry, the amount of atmosphere intercepted when viewing each pixel increases as the location of the pixel moves from the satellite subpoint toward the edge of the scan. The impact of increased pathlength alone, even in relatively dry atmospheric conditions, causes observed AVHRR brightness temperatures to become colder in cloud-free pixels. This phenomenon of increased atmospheric attenuation due solely to the pixel location has become known as limb darkening.

Corrections for limb darkening are typically made by applying the principles of radiative transfer theory, described above, to alter brightness temperatures to "expected temperatures" that would have been measured if the pixel were located at nadir. Such an approach uses some climatic information about the atmospheric composition (e.g., profiles of temperature, pressure, and gaseous absorbers) and the satellite sensor response functions, along with an atmospheric transmission model to estimate the reduction in brightness temperature due to atmospheric absorption. The result is that, prior to entering the automated cloud analysis algorithms, brightness temperatures might be raised by some "predefined" amount based upon imperfect knowledge of the real atmosphere.

A similar radiative transfer modeling approach has been used for the detection of optically thin cirrus clouds with automated cloud detection algorithms. The thresholds used to distinguish between cloud-free and cirrus cloudy pixels were derived from radiative transfer model calculations to define the threshold between optically thin cirrus and cloud-free pixels using BTD45, sensor scan angle, and channel 4 brightness temperatures, which are correlated with 117 different tropical and maritime atmospheres (SK 1988). However, there are several weaknesses with this approach including inaccuracies in atmospheric transmission modeling (Fleming et al. 1986) and errors related to applying calculations for a "model atmosphere" to areas of imagery with dissimilar atmospheric (water vapor) properties.

Any improved thin-cirrus detection algorithm must properly account for limb-darkening effects. Since atmospheric water vapor is primarily responsible for this phenomenon, it is reasonable to expect that the direct application of water vapor information, corrected for AVHRR sensor viewing geometry, could provide a more accurate correction than the use of radiative transfer modeling.

3. Results

a. *The threshold function concept*

In this research, we analyzed the impact of atmospheric water vapor on nighttime AVHRR infrared brightness temperatures and, in particular, the BTD35 feature, which has proved to be valuable for the detection of middle and high clouds, such as optically thin cirrus (SK 1988). More recently, the relationship between $TIWV_p$ and the BTD35 feature has been demonstrated to provide accurate pixel-level cloud decisions over variable scan angles and pathlengths (Hutchison et al. 1993). Furthermore, this approach relates limb-darkening effects to the primary phenomenon causing atmospheric attenuation (i.e., atmospheric water vapor) rather than a secondary cause [i.e., surface (skin) temperature].

Using NOAA AVHRR high-resolution (HRPT) imagery collected at the University of Texas Center for Space Research (UTCSR), and radiosonde data from the Lockheed Missiles and Space Company's Austin Division, coregistered conventional and satellite observations were collected for pixels that contained *very thin,* single-layered cirrus cloudy pixels and cloud-free pixel neighbors. The data were collected during the winter and summer months of 1992 and included

AVHRR imagery from the *NOAA-11* and *NOAA-12* sensors. The UTCSR ground station allows satellite data to be displayed in any spectral band while providing the ability to simultaneously interrogate a variety of data at each pixel, including pixel latitude, longitude, brightness temperatures in all AVHRR channels, sensor scan angle, and more. Data were collected for the area east of the Rocky Mountains using radiosonde sites from North Dakota to Texas and east to Cape Hatteras. After calculations were made of $TIWV_c$ from radiosonde observations, areas with weak horizontal water vapor gradients were identified as potential satellite data collection regions to compensate for temporal differences between the two datasets.

Optically thin cirrus clouds were manually identified in the HRPT imagery and all the aforementioned satellite data were recorded for a number of pixels representative of cirrus cloudy and cloud-free pixels in the region. Care was taken to ensure pixels were either cloud-filled or cloud-free. $TIWV_c$, calculated from radiosonde observations, were then corrected for satellite sensor viewing geometry. This path-dependent water vapor variable, $TIWV_p$, was entered into a database along with the satellite observations for further analysis.

Shown in Fig. 2 is the BTD35 feature as a function of $TIWV_p$ for cirrus cloudy and cloud-free pixels, respectively. (Note: $TIWV_p$ is shown in units of kilograms per square meter, which can be converted to precipitable centimeters upon dividing by 10.) It is apparent that the data separate into cloud-free and optically thin cirrus regions with a sharp distinction between them. The best fit to these data was taken as a line that approaches "BTD = 0" in a perfectly dry atmosphere and extends through the left edge of the data points for the optically thin cirrus clouds. This delineation has the form $BTD = 0.25 + 0.095TIWV_p$.

If the BTD35 is larger than values represented by the curve shown in Fig. 2, which we call the "threshold function," optically thin cirrus is nearly always present in the observations. If values are less than this curve, cloud-free conditions are nearly always present in the pixel.

With the same observations used in Fig. 2, the data were analyzed using the thin-cirrus test described by SK, which relies upon the BTD45 feature. By comparing the figures, it is apparent that the cirrus cloud signature is stronger in the BTD35 feature than the BTD45 feature, which demonstrates the higher sensitivity of the BTD35 feature for thin-cirrus detection.

b. Demonstration of the threshold function with an automated cloud analysis algorithm

The threshold function, depicted in Fig. 2, was implemented into an automated cloud analysis algorithm, where its performance for the improved detection of optically thin cirrus clouds was demonstrated on the multispectral image shown in Fig. 4. Panel a(2) shows the channel 5 image for this scene of optically thin cirrus collected by *NOAA-12* on 2 March 1992. The satellite overflew Austin, Texas, at about 0145 UTC, and the data extend from the Gulf coast north to St. Louis, which is in the upper-right corner. The image consists of cirrus and cloud-free pixels, except for the small stratus deck in the lower left, where some pixels contained both cirrus and stratus clouds. Panel a(1) shows the ground truth (cirrus) cloud analyses for the scene, which was created by manual analysis of the multispectral imagery. Unfortunately, some degradation was experienced in the AVHRR image during the reproduction process.

The manual (ground truth) analysis revealed that cirrus existed in 45.6% of the 1 048 576 scene pixels. Further analysis revealed that 14.8% of the pixels contained optically thick cirrus, defined by cloud-top temperatures at least as cold as the 400-mb temperature,

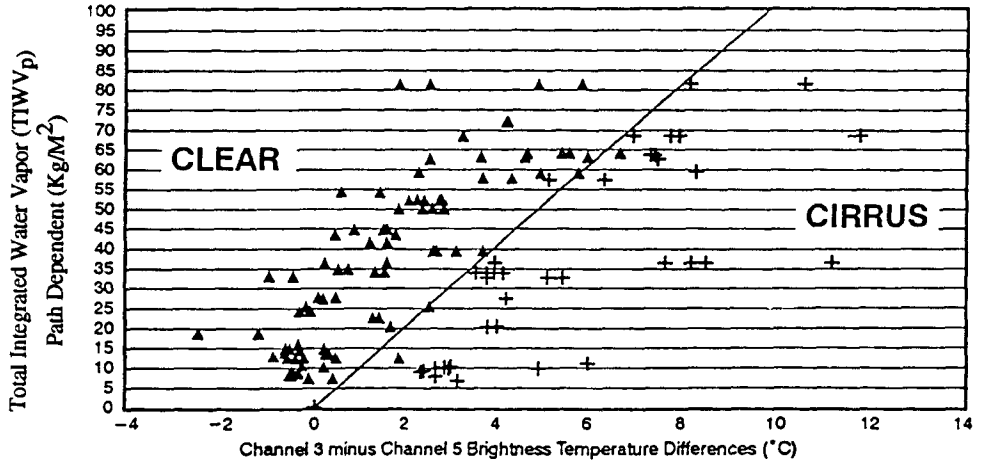

FIG. 2. Brightness temperature difference between AVHRR channels 3 and 5 versus path-dependent total integrated water vapor ($TIWV_p$) for cloud-free (▲) and cirrus cloudy (+) pixels.

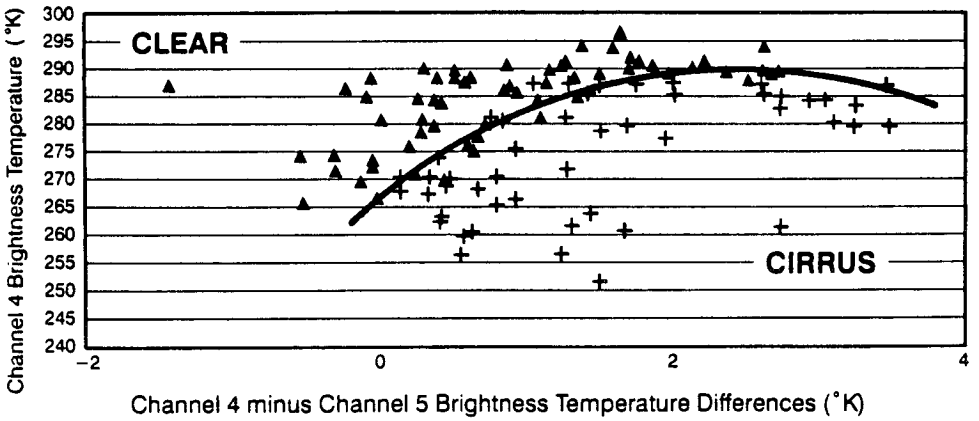

FIG. 3. Brightness temperature difference between AVHRR channels 4 and 5 versus channel 4 brightness temperature for cloud-free and cirrus cloudy pixels (after Saunders and Kriebel 1988).

leaving optically thin cirrus in 30.8% of the pixels. (While the term "optically thin cirrus" is normally associated with transmissivity or optical depth, distinction is made herein based upon cloud-top temperature only because pixels colder than this are readily classified as cirrus cloud contaminated and represent no difficulty in cloud detection.) The remaining 54.4% of the pixels were manually classified as cloud-free, which for the purposes of this demonstration included the small area of stratus in the lower left.

The automated cloud analysis algorithm performs cloud detection and/or cloud typing for a single test or group of tests. The output is a cloud/no-cloud analysis or a cloud-type analysis. For this particular case, the algorithm was run twice, each with a single test to detect optically thin cirrus. Panels b(1) and c(1) contain the automated cloud analysis of the multispectral data using results shown in Fig. 2 and the thin-cirrus test published by SK, respectively. The $TIWV_p$ analysis required to set the threshold function was based upon $TIWV_c$ calculated from 15 radiosondes that covered the region, which were then corrected for satellite viewing geometry. It was necessary to include a test to detect the optically thick cirrus clouds along with the thin cirrus, but further analyses distinguished between pixels classified by each cloud detection test. Differences between the automated and ground truth (manual) analyses are shown in panels b(2) and c(2), respectively.

Quantitative results show the SK thin-cirrus test [panels c(1) and c(2)] performed well and classified 84.7% of the pixels correctly when compared to the ground truth. However, the test identified only 18.7% of the optically thin cirrus compared with the 30.8% in the ground truth. Thus, the accuracy of the BTD45 feature for the detection of optically thin cirrus was only 60.7%. It is seen in panel b(2) that the thin-cirrus test failed to detect the outer edges (thinner parts) of the optically thin cirrus clouds contained in the ground truth.

The accuracy of the automated cloud analysis that used the BTD35 feature and $TIWV_p$ information [panels b(1) and b(2)] was 94.7%. Additionally, optically thin cirrus was detected in 28.1% of the pixels, compared with the 30.8% contained in the ground truth, for an accuracy of 91.2%. This represents an absolute improvement of 30.5% (91.2% − 60.7%) and more than a 50% relative improvement over the thin-cirrus test based only upon the BTD45 feature. Analyses of other scenes also showed similar results, but improvements were not as dramatic because the scenes did not have as much very thin cirrus as the scene shown in Fig. 4.

4. Discussion

The results shown in Figs. 2 and 4 show that the relationship between the BTD35 feature and $TIWV_p$ allows clear distinction between pixels that contain optically thin cirrus clouds from those that are cloud-free. Furthermore, the separation is less distinct with the BTD45 feature. The results agree with observational data shown in Figs. 2 and 3.

While these results are encouraging, the global applicability of the threshold function, shown in Fig. 2, awaits an assessment on the impact of surface reflections from downwelling radiance upon cloud spectral signatures. This contribution is described in the last term on the right-hand side of Eq. (1). Recent measurements suggest that the earth's surface reflects terrestrial radiation as a function of both soil type and wavelength (Salisbury and D'Aria 1992), which can also impact upwelling radiance at infrared wavelengths (Gao and Wiscombe 1994). Since surfaces in our study are seen to approximate blackbodies, for example, the BTD35 in a perfectly dry atmosphere approaches 0°, the threshold function may not be applicable over more gray surfaces, for example, sandy soils in desert areas, and the use of some land surface classification scheme will be required with the threshold function method-

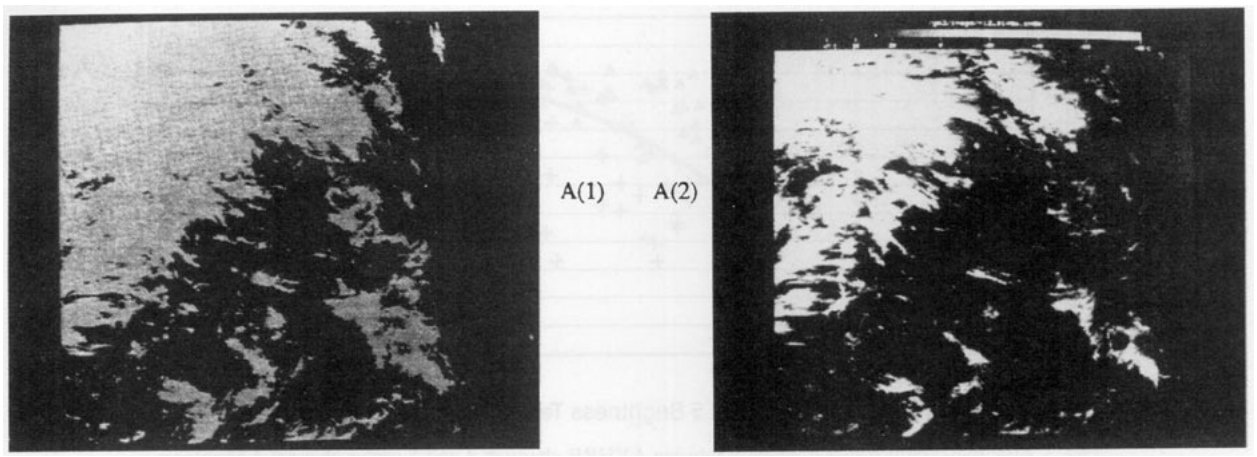

Panel A. A ground truth cirrus cloud (white), no cloud (black) analysis, A(1), of the NOAA-12 AVHRR Channel 5 imagery A(2).

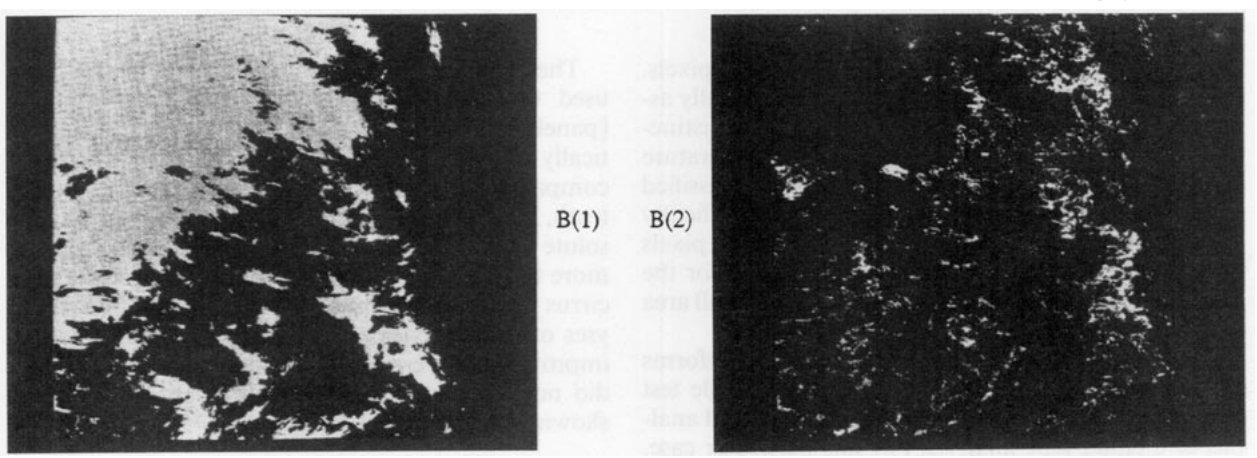

Panel B. Cloud, no cloud analysis of multispectral imagery using results from this research, B(1), along with differences between analysis and ground truth (shown in white), B(2).

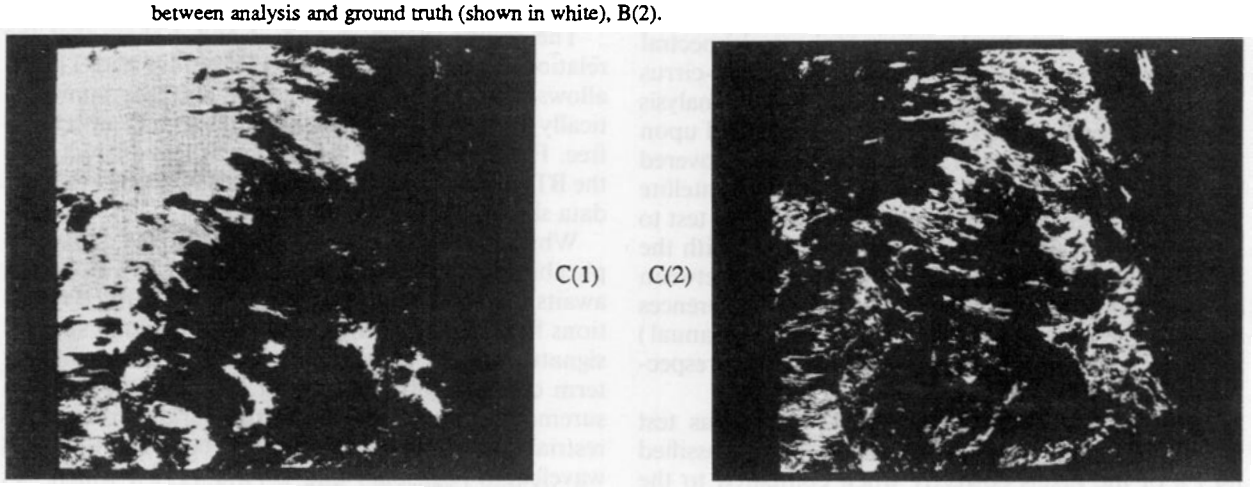

Panel C. Cloud, no cloud analysis based upon Saunders & Kriebel, C(1), and deviations from ground truth (in white), C(2).

FIG. 4. Analysis of optically thin cirrus over the southwestern United States for 2 March 1992.

ology. Further research is ongoing to quantify the impact of surface emissivity on thin-cirrus detection and define the need for a surface classification to extend this methodology toward a global application. In the meantime, the BTD45 feature continues to be highly valuable, especially with daytime imagery when solar energy contaminates the cirrus emissions at 3.7 μm.

The emissivity of cirrus has been shown to be highly variable and dependent upon wavelength (Inoue 1987; d'Entremont et al. 1990). Our simulations, shown in Fig. 5, demonstrate the relationship between the BTD35 feature and the emissivity of cirrus clouds. In a relatively dry atmosphere, the BTD35 may be small for very thin cirrus clouds, that is, clouds having a small emissivity. As the cirrus cloud optical depth and emissivity increases, the magnitude of the BTD35 feature also increases. However, as the cloud becomes optically thick, indicated by an emissivity that approaches unity, the BTD rapidly approaches zero. Thus, while the magnitude of the BTD35 feature can be used for the enhanced detection of optically thin cirrus clouds, it cannot be used to specify $TIWV_p$ in the presence of thin cirrus clouds without knowledge of the cloud emissivity and possibly the surface reflectivity.

The threshold function methodology may not detect optically thin cirrus in areas of reduced spectral signature, which can occur if thin cirrus and lower water clouds are both contained in the same pixel and when thin cirrus is found over cold surfaces. In such cases, the spectral signature of the cirrus cloud may be reduced below the detection threshold, since in the former the spectral signature of water clouds is opposite that of ice clouds (Hutchison et al. 1994a), while in the latter case there is simply less spectral signature to exploit. However, texture can be exploited in both of these cases to detect thin cirrus in areas of reduced spectral signature (Lameii et al. 1994).

The improved detection of thin cirrus is based on the knowledge and use of $TIWV_p$ in the vicinity of the thin cirrus clouds. For automated and operational cloud detection from satellite sensors, the $TIWV_p$ estimates should ideally also be obtained from satellite data. Fortunately, the Special Sensor Microwave/Imager (SSM/I) of the Defense Meteorological Satellite Program provides high quality estimates of $TIWV_c$ over ocean surfaces. Thus, it is expected that this thin-cirrus detection methodology, which has been developed and tested using radiosonde data, will perform equally well with $TIWV_p$ estimates derived from the SSM/I sensor. This approach has been tested on limited datasets (Hutchison et al. 1994b). It is postulated that $TIWV_c$ values from numerical modeling may allow the use of the threshold function methodology over land surfaces in an operational environment. However, this remains to be evaluated.

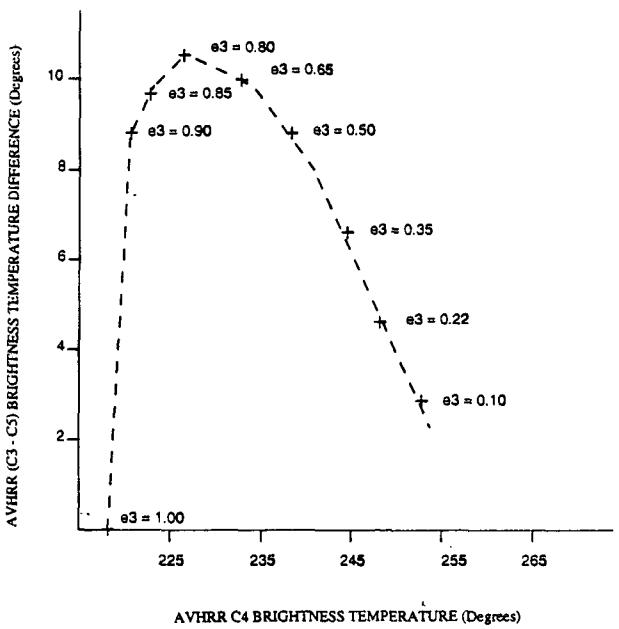

FIG. 5. Simulated AVHRR channels 3 minus 5 brightness temperature differences for cirrus clouds of variable thickness.

5. Summary

A relationship has been defined that incorporates atmospheric attenuation due to water vapor into the automated detection of optically thin cirrus in nighttime multispectral satellite imagery. The relationship based upon the BTD35 feature and $TIWV_p$ allows clear distinction between optically thin cirrus cloudy pixels and cloud-free pixels. Additionally, this multivalued relationship, which we refer to as a threshold function, provides improved sensitivity for the detection of optically thin cirrus when compared with the BTD45 feature.

Acknowledgments. The research was conducted with the indispensable assistance of Dr. Melba Crawford at the University of Texas, Center for Space Research, who graciously provided access to the NOAA High Resolution Picture Transmission (HRPT) Ground Station and library of imagery data.

REFERENCES

Coakley, J. A., and F. P. Bretherton, 1982: Cloud cover from high-resolution scanner data: Detecting and allowing for partially filled fields of view. *J. Geophys. Res.*, **87**, 4917–4932.

d'Entremont, R. P., M. K. Griffin, and J. T. Bunting, 1990: Retrieval of cirrus radiative properties and altitudes using multichannel infrared data. Preprint, *Fifth Conf. on Satellite Meteorology and Oceanography*, London, United Kingdom, Amer. Meteor. Soc., 4–9.

Fleming, H. E., D. S. Crosby, and A. C. Neuendorffer, 1986: Correction of satellite temperature retrieval errors due to errors in atmospheric transmittances. *J. Climate and Appl. Meteor.*, **25**, 869–882.

Gao, B.-C., and W. J. Wiscombe, 1994: Surface-induced brightness temperature variations and their effects on detecting thin cirrus clouds using IR emission channels in the 8–12-μm region. *J. Appl. Meteor.*, **33**, 568–570.

Hutchison, K. D., J. Mack, R. McDonald, and G. Logan, 1991: The positive identification of optically-thin cirrus in nighttime, multispectral meteorological satellite imagery by automated clouds detection and typing algorithms. *Proc. on the Cloud Impacts on DoD Operations and Systems 1991 Conf.*, Los Angeles, CA, Air Force Phillips Laboratory, 305–309.

——, ——, G. Logan, K. R. Hardy, and S. Westerman, 1993: Identification of optically-thin cirrus clouds by automated classifi-

cation algorithms using multispectral, multisensor meteorological satellite data. *Proc. SPIE 93-Passive IR Remote Sensing of Clouds and the Atmosphere. I,* Orlando, FL, Soc. Photo-Opt. Instrum. Eng., 240–243.

——, ——, K. Hardy, and S. Westerman, 1994a: The automated classification of optically-thin cirrus and stratus clouds in nighttime AVHRR imagery using water vapor derived from the DMSP SSM/I sensor. Preprints, *Seventh Conf. on Satellite Meteorology,* Monterey, CA, Amer. Meteor. Soc., 291–294.

——, ——, ——, and ——, 1994b: The application of total integrated water vapor content derived from DMSP SSM/I data for enhanced automated cloud detection in multispectral meteorological satellite imagery. Preprints, *Eighth Conf. on Atmospheric Radiation,* Nashville, TN, Amer. Meteor. Soc., 403–405.

Inoue, T., 1985: On the temperature and effective emissivity determination of semi-transparent cirrus clouds by bi-spectral measurements in the 10 micron window region. *J. Meteor. Soc. Japan,* **63,** 88–99.

——, 1987: A cloud type classification with *NOAA-7* split-window measurements. *J. Geophys. Res.,* **92,** 3991–4000.

Karlsson, K.-G., and E. Liljas, 1990: The SMHI Model for cloud and precipitation analysis from multispectral AVHRR data. SMHI Promis-Rapporter Nr 10, August 1990, Promis Reports, 74 pp.

Key, J., J. A. Maslanik, and A. J. Schweiger, 1989: Classification of merged AVHRR and SMMR arctic data with neural networks. *Photo. Eng. Remote Sens.,* **55,** 1331–1338.

Kneizys, F. X., E. P. Shettle, L. W. Abreu, J. H. Chetwynd, G. P. Anderson, W. O. Gallery, J. E. A. Selby, and S. A. Clough, 1988: Users guide to LOWTRAN 7. AFGL TR-88-0177, Air Force Geophysics Laboratory.

Lameii, N., K. D. Hutchison, and M. M. Crawford, 1994: Cloud type discrimination via multispectral textural analysis. *J. Opt. Eng.* **33,** 1303–1313.

Liou, K.-N., 1980: *An Introduction to Atmospheric Radiation.* Int. Geophys. Series, Vol. 26, Academic Press, 392 pp.

Salisbury, J. W., and D. M. D'Aria, 1992: Emissivity of terrestrial materials in the 8–14 micron atmospheric window. *Remote Sens. Environ.,* **42,** 83–106.

Saunders, R. W., and K. T. Kriebel, 1988: An improved method for detecting clear sky and cloudy radiances from AVHRR data. *Int. J. Remote Sens.,* **9,** 123–150.

Stowe, L. L., E. P. McClain, R. Carey, P. Pellegrino, G. G. Gutman, P. Davis, C. Long, and S. Hart, 1991: Global distribution of cloud cover derived from NOAA/AVHRR operational satellite data. *Adv. Space Res.,* **11,** 51–54.